Imidazolium-based titanosilicate nanospheres as active catalysts in carbon dioxide conversion

Comès, Adrien; Poncelet, Rémy; Pescarmona, Paolo P.; Aprile, Carmela

Published in:
Journal of CO2 Utilization

DOI:
10.1016/j.jcou.2021.101529

Publication date:
2021

Journal of CO2 Utilization 48 (2021) 101529

Contents lists available at ScienceDirect

Journal of CO2 Utilization

journal homepage: www.elsevier.com/locate/jcou

Imidazolium-based titanosilicate nanospheres as active catalysts in carbon dioxide conversion: Towards a cascade reaction from alkenes to cyclic carbonates

Adrien Comès [a], Rémy Poncelet [a], Paolo P. Pescarmona [b], Carmela Aprile [a,*]

[a] Laboratoire de Chimie des Matériaux Appliqués, Département de Chimie, Université de Namur, Rue de Bruxelles, 61, 5000, Namur, Belgium
[b] Chemical Engineering Group – Engineering and Technology Institute Groningen (ENTEG), University of Groningen, Nijenborgh 4, 9747 AG, Groningen, the Netherlands

ARTICLE INFO

Keywords:
Titanosilicates
Carbon dioxide conversion
Epoxidation
Mesoporous particles
Imidazolium salt

ABSTRACT

Porous silica-based nanospheres bearing titanium centres as single site were successfully synthesized employing a time- and energy-efficient procedure. The influence of the post-synthesis treatment on the insertion of Ti was investigated via DR UV–Vis and XPS spectroscopy and the titanium content was quantified through ICP-OES analysis. The textural and structural properties of the different solids were evaluated via XRD, TEM and N_2 physisorption. The resulting materials were thereafter covalently functionalized with imidazolium chloride, followed by characterization via ^{29}Si and ^{13}C solid-state NMR, N_2 physisorption and chemical combustion analysis. The bi-functional catalysts were tested in the challenging conversion of CO_2 with cyclohexene oxide to the corresponding cyclic carbonate as well as with various other epoxides with excellent results. The insertion of Ti as single site played a key role substantially improving the activity of the solids. The most active bi-functional material was successfully recovered and reused through multiple cycle without loss of the catalytic activity. Moreover, the cyclohexene epoxidation reaction was tested as well employing the mono-functionalized Ti-based material. The catalytic mixture, composed by the mono-functional and bi-functional solids, was efficiently used to convert the cyclohexene into cyclohexene oxide and subsequently the cyclohexene oxide into the corresponding carbonate thus opening the prospect for a cascade reaction.

1. Introduction

In 1998, Anastas and Warner proposed a conceptual breakthrough in science establishing 12 principles toward a more sustainable chemistry [1,2]. These green chemistry principles focus on the development of novel strategies and synthetic pathways that employ non- or less toxic chemicals as well as less energy intensive and more environmentally friendly processes. In this context, catalysis is one of the key pillars of sustainability. Hence, the design of active and selective catalysts that are able to efficiently promote reactions and ensure a low environmental factor is constantly drawing the attention of the scientific community [3,4]. Heterogeneous catalysts are particularly attractive due to their possible recover from the reaction medium and reuse in multiple cycles. Many industrial processes such as ammonia synthesis [5] or the Ziegler-Natta [6] polymerization, rely on the use of solid-state catalysts. Micro- and mesoporous materials such as zeolites, as well as properly functionalized MCM-41 [7,8], MCM-48 [7,8], SBA-15 [9] are extensively employed in the field of heterogeneous catalysis [10,11]. The broad range of application of these solids is related to the easy tuneability of their catalytic properties via isomorphous substitution of silicon with various metal cations, the possibility of impregnation procedures as well as the covalent functionalization of the surface together with their elevate specific surface area, modulable porosity and high robustness from chemical, physical and mechanical point of view. In particular, an interesting feature of the mesoporous silica-based materials is the possibility to insert heteroatoms (i.e. different from silicon) as single sites [10]. This can be performed via co-synthesis or post-synthesis strategies. By co-synthesis approach, the heteroatom and the silica precursors are mixed together in a one-step reaction [12–15]. Post-synthesis is generally a two-step procedure involving the synthesis of the solid support followed by the grafting of the heteroatom on the surface [16–19].

One of the most studied transition metal cations is represented by titanium. The TS-1 is largely employed at industrial scale for the

* Corresponding author.
E-mail address: carmela.aprile@unamur.be (C. Aprile).

https://doi.org/10.1016/j.jcou.2021.101529
Received 16 December 2020; Received in revised form 30 March 2021; Accepted 4 April 2021
Available online 16 April 2021

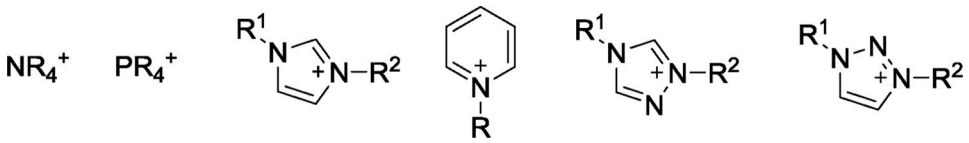

Scheme 1. General representation of several cations. From left to right: ammonium, phosphonium, imidazolium, pyridinium, 1,2,4-triazolium and 1,2,3-triazolium.

epoxidation of alkenes but it suffers from pore size limitation [20,21], while Ti-MCM [22–24] and Ti-SBA [25–27] and Ti-TUD, have larger pores that allow working with bulkier alkenes.

Due to their Lewis acid properties, Ti-based silicates are employed in a plethora of reactions [28,29] including alkenes epoxidations [21–27, 30,31], epoxide isomerization to aldehyde [32], glycerol acetalization [33] or sugar isomerization [34].

Lewis acids are often used in the conversion of carbon dioxide into (cyclic)carbonates. They are mostly employed as co-catalysts for the reaction between CO_2 and epoxides, in combination with various catalysts as ammonium [35], phosphonium [36,37], imidazolium [38,39], pyridinium [40,41] or triazolium [42,43] salts (Scheme 1) [44]. It is generally accepted that epoxides can be activated via coordination of the oxygen at three-membered ring with a Lewis acid site, thus facilitating the ring opening via nucleophilic substitution (usually from the counterion of the salt) and decreasing the energy consumption [45].

Various solids with Lewis acid character were already developed and tested under heterogenous conditions often in the presence of tetrabutylammonium bromide or iodide in homogeneous phase [46–50]. Few researches describe the synthesis of a material containing both the Lewis acid and the ammonium or imidazolium salts in heterogeneous phase. One of the first report published by North and co-workers involves the grafting, through an ammonium-based linker, of a bimetallic aluminium (salen) complex [51–54]. Sadeghzadeh proposed the covalent anchoring of the efficient imidazolium cation combined with the phosphotungstic acid derivative $H_2PW_{12}O_{40}^-$ as clusters active through the coordination of the epoxides [55]. Latest strategies use various metal-organic frameworks (MOF) as Lewis acid source. Some authors reported the synthesis of MOF using a modified terephthalic acid on which trimethylammonium iodide [56], tributylammonium bromide [57] or imidazolium bromide [58,59] is anchored by post-functionalization. Other authors used terephthalic acid modified by imidazolium salt as direct organic building unit for the MOF synthesis [49,60]. Recently, Ding and Jiang proposed an encapsulation of a poly-imidazolium salt inside the MOF porous structure [61].

Similarly, we also reported the synthesis of a porous material with Lewis acid inserted as single site in the silica architecture and post-functionalized by an imidazolium salt [62]. More recently, we described the synthesis of a tri-functional heterogeneous catalyst bearing imidazolium salts decorated with alcohol functionalities anchored on a porous support embedding Sn as single site to play the role of Lewis acid centre [63].

Herein, we report a fast and energy saving approach for the synthesis of porous titanosilicate nanospheres requiring only 1 h reaction time without additional hydrothermal treatment under static conditions. The post-synthesis treatment for removal of the template was also evaluated. The solids were decorated with imidazolium salts in order to generate a bi-functional heterogeneous catalyst able to efficiently promote the synthesis of cyclic carbonates via CO_2 conversion. Titanium is expected to be a better co-catalyst than the previously reported Sn- and Zn-based solids due to its higher affinity for the oxygen. The solids were extensively characterized via various techniques, including transmission electron microscopy (TEM), X-ray diffraction (XRD), N_2-physisorption, X-ray photoelectron spectroscopy (XPS), UV–Vis diffuse reflectance (DR UV–Vis), inductively coupled plasma optical emission spectroscopy (ICP-OES), ^{29}Si- and ^{13}C-CP MAS NMR. Their catalytic performances were evaluated in the reaction between epoxides and CO_2 to form the corresponding cyclic carbonates. The materials revealed excellent catalytic performances displaying high turnover numbers and turnover frequencies even in the challenging synthesis of cyclohexene carbonate. Moreover, the unfunctionalized material was also active in the conversion of cyclohexene to cyclohexene oxide, thus proving the versatility of the synthesis approach.

2. Experimental section

2.1. Materials and methods

Ammonium hydroxide (30 %), fuming hydrochloric acid and acetonitrile were purchased from Carl Roth GmbH + Co. Cetylmethylammonium bromide (CTAB), tetraethylorthosilicate (TEOS), tetraisopropylorthotitanate, N-methylimidazole, (3-chloropropyl) trimethoxysilane, styrene oxide, cyclohexene oxide, epichlorohydrin and tert-butyl hydroperoxide (70 % in water) and were purchased from TCI NV Europe. Glycidol, 1,2-epoxybutane, cyclohexene and mesitylene were purchased from Sigma-Aldrich. DMSO-d6 was purchased from Eurisotop. All chemicals were used as received without further purification. Milli-Q water was 18.2 MΩ.cm.

^{29}Si and ^{13}C NMR spectra were recorded at room temperature on a Bruker Avance-500 spectrometer operating at 11.7 T (99.3 MHz for ^{29}Si and 125.7 MHz for ^{13}C) using a 4 mm CP-MAS Bruker probe. The sample were packed in a zirconia rotor and measured with spinning frequencies of 8000 Hz. Cross polarization CP-MAS spectra were recorded using a 5 s relaxation delay and 5 ms contact time for ^{29}Si and 2 ms for ^{13}C. Quantitative ^{29}Si spectra were recorded using a 300 s relaxation delay, a 3 µs excitation pulse and a 52 ms acquisition time. The processing comprised exponential multiplication of the FID with a line broadening factor of 30 Hz for ^{29}Si or 10 Hz for ^{13}C, zerofilling, Fourier transform, phase and baseline corrections. The chemical shift scale was calibrated at room temperature with respect to a sample of solid 3-(trimethylsilyl)-1-propanesulfonic acid sodium salt (DSS) (0.0 ppm).

Nitrogen adsorption-desorption analyses were carried out at liquid nitrogen temperature with a volumetric adsorption analyser (Micromeritics ASAP2420). Prior to the analysis, the samples were pre-treated in two steps (90 °C for 1 h and 150 °C for 8 h) under reduced pressure (<10 mTorr). The Brunauer–Emmet–Teller (BET) method was applied in the 0.05–0.30 relative pressure range to calculate the specific surface area, while the pore size distributions were determined by BJH and DFT method, using cylinder geometry, N_2 – Cylindrical Pores – Oxide surface model, 0.10 regularization and a version 2 deconvolution.

Transmission electron microscopy (TEM) images were obtained using a Philips Tecnai 10 microscope operating at 80 kV. Samples were prepared by dispersion of a small quantity of material in absolute ethanol and deposited onto a copper grid.

The X-ray photoelectron spectroscopy (XPS) analyses were performed on a ThermoFisher ESCALAB 250Xi instrument. This spectrometer uses a monochromatic Al Kα X-ray source (1486.6 eV) and a hemispherical deflector analyser (SDA) working at constant pass energy (CAE). This mode allows a constant energy resolution on the whole spectrum. The intrinsic resolution of the spectrometer is 0.47 eV, measured on the Ag $3d_{5/2}$ line. The experiments were performed using a 300 µm diameter X-ray spot. The charge neutralization of the sample was achieved with a flood gun using low energy electrons and Ar^+ ions. The base pressure in the analyser chamber was 2.10^{-8} Pascal, and during experiments an argon partial pressure of 3.10^{-5} Pascal was maintained for the flood gun operation. Survey spectra were recorded

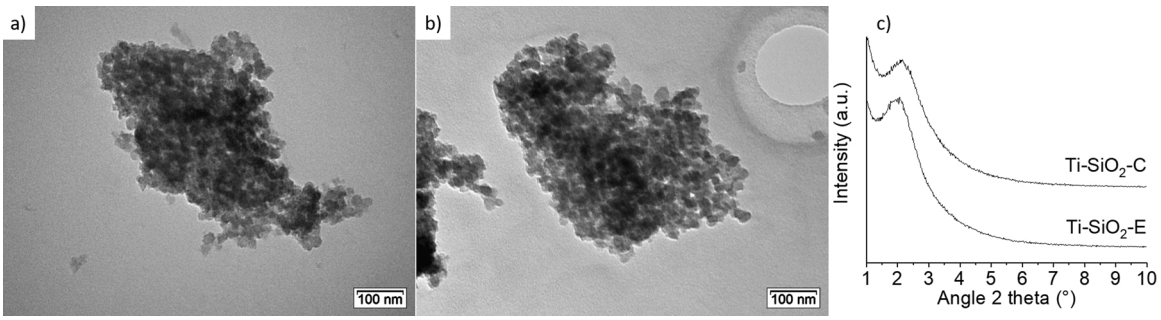

Fig. 1. TEM pictures of Ti-SiO_2-E (a) and Ti-SiO_2-C (b) and the corresponding low-angle XRD (c).

with a 150 eV pass energy, and this energy was decreased to 25 eV for high-resolution spectra.

Diffuse reflectance UV–vis spectra were recorded with a Varian Cary 5000 UV–Vis-NIR Spectrophotometer.

Inductively coupled plasma optical emission spectroscopy (ICP-OES) employed to determine the chemical composition of the materials was performed an Optima 8000 ICP-OES Spectrometer. Digestion was performed weighting 10 mg of the solid and digesting it with aqua regia (100 µL) and hydrofluoric acid (600 µL) in 10.0 ml milli-Q water. Ti (1000 mg/L) standard solution, nitric, hydrochloric and hydrofluoric acids Ultra-quality for calibration and digestion steps were purchased from Carl Roth GmbH.

Chemical combustion analyses were performed on a Perkin-Elmer 2400 Serie 2 analyser.

^{1}H NMR spectroscopy of liquid samples was performed on a JEOL ECA operating at 9.4 T (400 MHz).

2.2. Synthesis of Ti-SiO_2 solids

Mesoporous silica-based materials were prepared adapting a previously reported dilute route [13,64]. Ammonium hydroxide (1.422 mL, 10.95 mmol) and CTAB (1.516 g, 4.16 mmol) were dissolved in 726 ml of distilled water. When a clear solution was obtained, TEOS (6.936 g, 33.29 mmol) and tetraisopropylorthotitanate (132 µL, 0.45 mmol) were mixed together and added dropwise in the aqueous solution. After 1 h under vigorous stirring at room temperature, the solid was filtered and washed 3 times alternatively with water and ethanol. The solid was dried overnight at 65 °C. It was then submitted to calcination and/or extraction respectively described here after. The calcination was performed in a Nabertherm oven with heating and cooling rate of 120 °C/h under air for 8 h at 550 °C. The extraction was performed dispersing the solid (3 g) in ethanol (200 mL) and adding HCl (24 mL) under stirring [65]. After 4 h under agitation at 50 °C, the solution was filtered and washed by ethanol until the pH of the filtrate was neutral. The recovered solid was dried at 100 °C.

2.3. Synthesis of Ti-SiO_2-imi [62]

The Ti-SiO_2 solid was dried in oven at 100 °C overnight before functionalisation. In a round bottom flask, the silica matrix (1.5 g) was suspended in 15 ml of dry toluene. Under agitation, N-methylimidazole (24 mmol) and (3-chloropropyl)trimethoxysilane (12 mmol) were added. The mixture was stirred at reflux temperature for 24 h. After cooling, the material was washed with Soxhlet extractor using ethanol as solvent.

2.4. Catalytic tests: conversion of epoxides and CO_2

All catalytic tests were performed in a *Cambridge Design Bullfrog* batch reactor. All catalysts were dried overnight at 100 °C prior to catalytic test. In a typical test, the solid was weighted in a Teflon vial of 0.15 L. The epoxide (24 mL) was added without solvent. Then, the reactor was closed, purged with a gentle flow of N_2 for 10 min, pressurized with CO_2 (25 bar) and heated. The mixture was stirred at 500 rpm using PTFE-coated mechanical stirrer. At the end of the reaction, the reactor was cooled down to room temperature, the pressure released and the reactor opened. The reaction mixture was submitted to centrifugation for 10 min at 4500 rpm and the supernatant was analysed by ^{1}H-NMR using DMSO-d6 as solvent.

2.5. Catalytic tests: epoxidation

All catalysts were dried overnight at 100 °C prior to catalytic test. In a typical test, the solid was weighted in a 20 ml glass vial. The solvent (4.5 ml acetonitrile), the internal standard (50 µL mesitylene), the alkene (4.5 mmol cyclohexene) and the oxidant (4.5 mmol $TBHP_{aq}$) were added. The vial was closed with a silicon/PTFE screw cap and heated at 70 °C using dry heating block. The mixture was stirred at 500 rpm using cross-shaped PTFE-coated magnetic stirrer. The mixture was analysed on a Trace 1300 gas chromatograph from Thermo Scientific equipped with a Rt-Q-Bond column (15 m long, 0.25 mmID, 8 µmdf) from Restek. The inlet was preheated at 250 °C. The oven sequence was the following: 50 °C for 1 min, heating ramp of 50 °C/min up to 250 °C and a plateau at 250 °C for 5 min. The carrier gas was N_2 flowing at 1 mL/min. The instrument was equipped with a flame ionization detector (FID) powered by a mixture of H_2 and dry air.

3. Results and discussion

3.1. Materials synthesis and characterization

The synthesis of mesoporous titanosilicate nanospheres was accomplished via an optimized diluted protocol adapting a previously reported methodology [13,64]. The material was prepared using a co-synthesis strategy involving the hydrolysis and condensation of titanium and silicon alkoxides in basic medium and in the presence of cetyltrimethymammonium bromide (CTAB) as structure directing agent. It should be mentioned that the optimized procedure implies a short synthesis time (1 h) and allows obtaining the porous solids without additional hydrothermal treatments under static conditions hence improving the sustainability of the whole procedure. After the synthesis, in order to ensure the removal of the surfactant and thus make the pores accessible, the solid was subjected to two different treatments: calcination or extraction in acidic ethanol [65,66]. These two methods were selected to investigate the influence of the post-synthesis treatment on the insertion of titanium as single site. The two materials were respectively labelled as **Ti-SiO_2-C** (where C stands for calcined) and **Ti-SiO_2-E** (where E stands for extracted). The structural and textural properties of both materials were initially investigated through transmission electron microscopy (TEM) and X-Ray Diffraction (XRD). TEM analysis of the samples (Fig. 1a and b) revealed that all the particles display an almost spherical shape with very small size (compared to standard

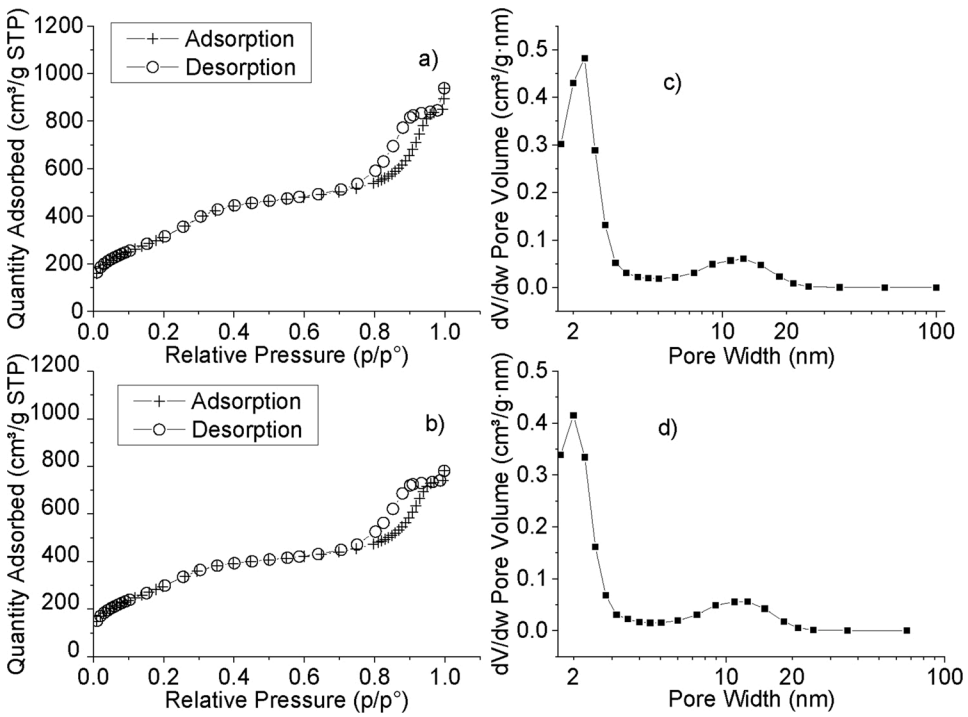

Fig. 2. N_2-physisorption isotherms (left) and BJH pore size distribution (right) of Ti-SiO_2-E (a; c) and Ti-SiO_2-C (b; d). Pore size distribution are presented using a logarithmic scale.

Table 1
Textural and structural properties of the synthesised titanosilicates.

Entry	Material	BET Surface Area (m^2/g)	Pore Size (nm) [a]	Ti inserted (mg/g) [b]
1	Ti-SiO_2-C	1140	3.1	12.4
2	Ti-SiO_2-E	1198	3.3	7.7
3	Ti-SiO_2-CE	1204	3.0	8.8

[a] Determined by DFT method.
[b] Amount of Ti determined via ICP-OES and expressed in mg of Ti per gram of material.

MCM-41-like solids) and a narrow particle size distribution centred at 30 nm.

To the best of our knowledge this precise control of the size below 100 nm was never reported previously. The regular arrangement of the pores was assessed through low-angle XRD (Fig. 1c). Both samples present a main contribution at c.a $2\theta = 2.1^\circ$ which can be assigned to a d_{100} diffraction [12–14,67]. The broadness of the signal is not surprising and can be related to the small size of the particles and the consequent decrease of long-range order [14,64].

Nitrogen physisorption analysis (isotherms presented in Fig. 2) allows confirming the mesoporosity and the elevate surface area of the solids. Both **Ti-SiO_2-C** and **-E** display a high specific surface area of 1140 m^2/g and 1198 m^2/g, respectively. A deep investigation of the pore size distribution via both BJH (Fig. 2) and DFT methods (Figure S1) showed the presence of a bimodal distribution. The first one, around 3.2 ± 0.2 nm as determined by DFT [68], is characteristic of materials with small-mesopores like MCM-41. The second and broader one, (centred at 13 nm) visible on the BJH pore size distribution, is the result of the reduced size of the particles and a consequence of the inter-granular space [13,14,64]. Chemical combustion analysis revealed that both extraction in HCl/EtOH and calcination procedures are efficient to ensure the complete removal of the templating agent. N_2 physisorption of the solid before calcination or extraction is presented in Supplementary Material (Figure S2).

The results discussed so far showed no relevant differences in textural and structural properties between the materials obtained via extraction or calcination procedure.

The amount of titanium in the materials was measured by ICP-OES analysis (Table 1, Entries 1–2) while its insertion as single site was assessed through both DR UV–Vis and XPS spectroscopies (Fig. 3). ICP-OES analysis of the samples (Table 1, entries 1–2) allowed evidencing a first significant difference between the two solids. Ti-SiO_2-C displays a much higher titanium loading than the corresponding solid obtained via extraction.

DR UV–Ais analysis of titanosilicates are profusely described in literature. The different absorption bands are directly correlated to the isomorphic substitution of silicon with titanium in the SiO_2 architecture as well as to the formation of extra-framework domains. The bands between 215 and 230 nm are usually attributed to Ti species in a (distorted) tetrahedral environment, while a shift at higher wavelength (around 270 nm) is ascribed to pentacoordinated surface species most probably in interaction with water molecules. A further shift towards the UV—A (290 nm) is associated to the formation of octahedral oligomeric chains and the contribution above 300 nm is attributed to TiO_2 domains. **Ti-SiO_2-E** displays a band centred at 230 nm corresponding to the expected tetrahedral environment [23]. The larger peak observed for **Ti-SiO_2-C** (ranging from 230 and 290 nm) suggests the presence of a combination of different Ti-based species, most probably as tetra-, penta- and hexa-coordinated sites [69]. From these results, it emerged clearly that the calcination used to remove the template has a detrimental effect on the insertion of Ti as single site. This behaviour could be ascribed to a migration (favoured by the high temperature) of the Ti species on the external surface with the consequent formation of a mixture of different extra-framework structures. It is possible that the small size of the particle contributes to the efficiency of the migration. In order to understand if the process could be at least partially reversible, the **Ti-SiO_2-C** solid was submitted to the same acid extraction applied to **Ti-SiO_2-E**. The resulting materials which underwent both calcination and extraction treatments was named **Ti-SiO_2-CE**. The full characterization of the solid can be found in Supplementary Material (Figures S3).

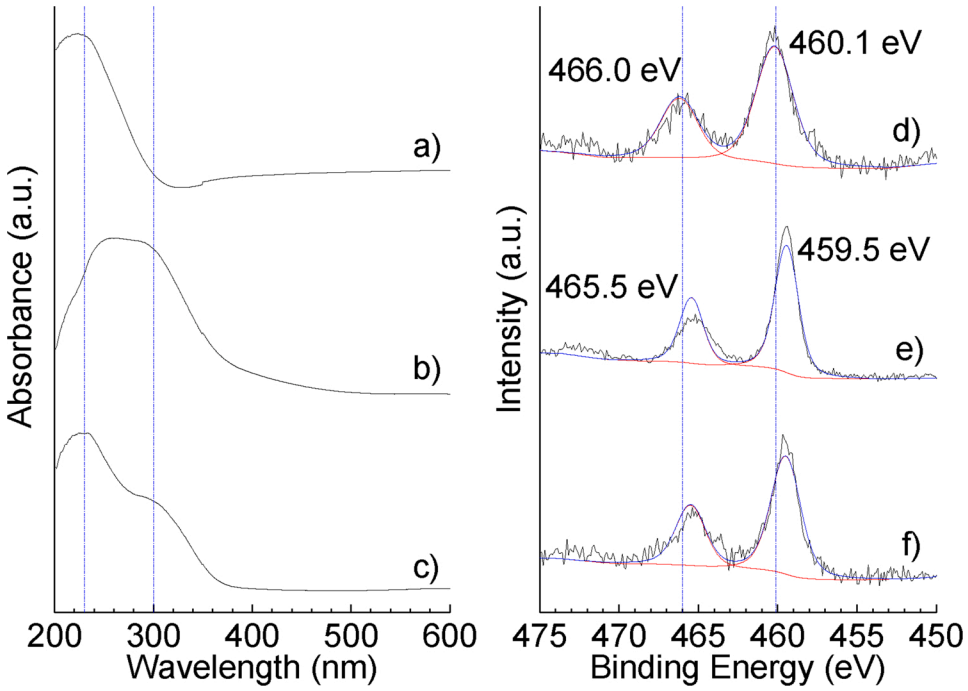

Fig. 3. DR UV–Vis (left) and XPS (right) of Ti-SiO_2-E (a; d); Ti-SiO_2-C (b; e) and Ti-SiO_2-CE (c; f). Vertical guidelines in UV–Vis spectra are positionned at 230 nm and 300 nm. Vertical guidelines in XPS are centred on the peaks of Ti-SiO_2-E to underscore the shift of Ti-SiO_2-C and –CE.

The UV–Vis spectrum is shown in Fig. 3. As can be seen, the sample **Ti-SiO_2-CE** exhibits two more defined maxima (compared to **Ti-SiO_2-C**) at 230 nm and 300 nm. Moreover, the band at higher wavelength is less pronounced suggesting a partial conversion of the pentahedral or isolated octahedral species in tetrahedral sites [26,70–72]. However, this modification of the UV–Vis pattern, could be also associated to a leaching of oligomeric surface titanium oxide chains in the acidic solution. In order to support or exclude this hypothesis, ICP-OES analysis of the **Ti-SiO_2-CE** solid was performed as well. The ICP-OES data (Table 1, Entry 3) showed a decrease in the amount of Ti corresponding to c.a. 25 % of the initial value (determined for **Ti-SiO_2-C)** thus indicating a possible leaching in solution. These experiments were performed in duplicate with highly reproducible results, thus proving the robustness of the whole process of synthesis and templating agent removal.

The conclusions derived from the analysis of the DR UV–Vis spectra were supported by XPS analysis (Fig. 3). The 2p core level XPS spectra on Fig. 3 displays the typical doublets in the region between 455 and 470 eV (with a separation of 5.75 eV) which are assigned respectively to Ti $2p_{3/2}$ and Ti $2p_{1/2}$ components originating from the spin–orbit splitting effect contributions. It is known that TiO_2 in octahedral coordination displays a doublet in which the most intense contribution is located at 458.5 eV (Figure S4). As can be clearly seen in the Fig. 3, the Ti $2p_{3/2}$ contribution in **Ti-SiO_2-E** displays an evident shift (1.5 eV difference) at higher binding energy. According to literature, this shift can be attributed to a different chemical environment of Ti that is mainly present in tetrahedral coordination [73–75]. The Ti $2p_{3/2}$ binding energy of **Ti-SiO_2-C** and **Ti-SiO_2-CE** present intermediate values between **Ti-SiO_2-E** and TiO_2 indicating that a combination of different Ti species is most probably present. These results are in agreement with the previous finding and allow confirming the detrimental effect of the calcination process on the insertion of Ti as single site in the silica network.

From the previous characterization, **Ti-SiO_2-E** emerges as the most promising material for further functionalization. However, to go in depth in our analysis, all the Ti-based silicates were decorated with imidazolium moieties following a one-pot procedure previously described by us [62]. The presence of the organic moieties as well as the covalent nature of the functionalization were addressed respectively via ^{13}C and ^{29}Si solid-state NMR. The two aromatic signals at 140 ppm and

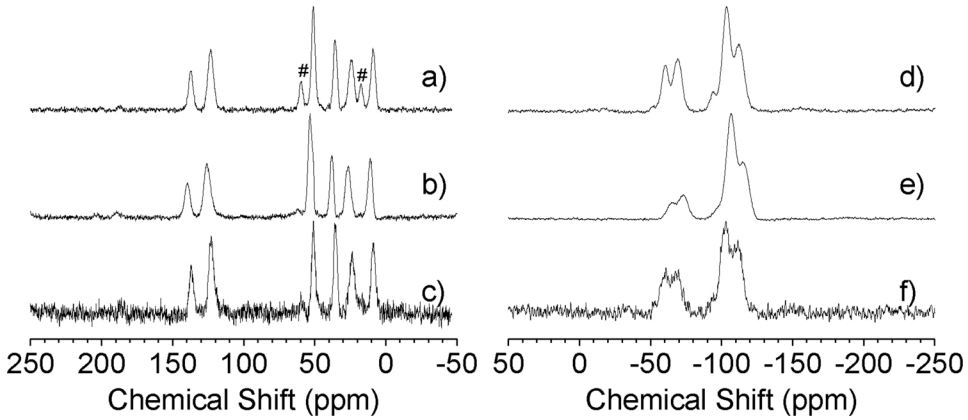

Fig. 4. ^{13}C CP MAS NMR (left) and ^{29}Si CP MAS NMR (right) of Ti-SiO_2-E-imi (a; d); Ti-SiO_2-C-imi (b; e) and Ti-SiO_2-CE-imi (c; f). The symbol # indicates some contribution related to the residual ethanol employed during washing procedures.

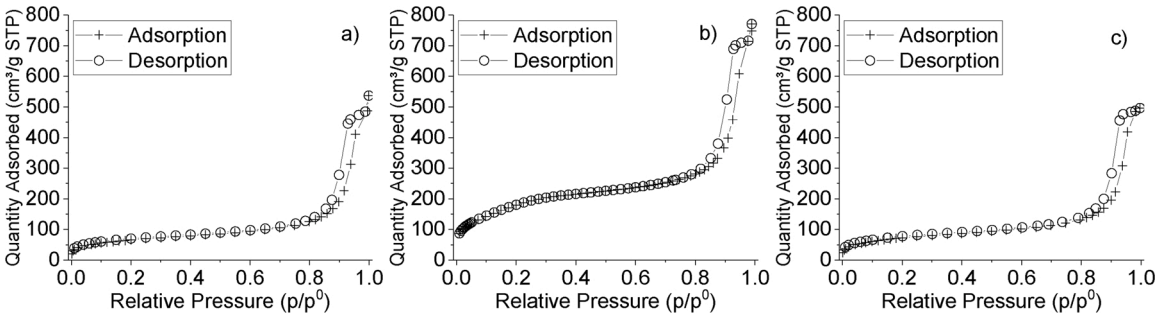

Fig. 5. N_2-physisorption isotherms of Ti-SiO_2-E-imi (a); Ti-SiO_2-C-imi (b) and Ti-SiO_2-CE-imi (c).

Table 2
Textural and structural properties of the catalysts.

Entry	Material	Amount of imidazolium (mmol/g) [a]	BET surface area (m^2/g)	Pore size distribution (nm) [b]
1	Ti-SiO_2-C-imi	1.04	669	2.7
2	Ti-SiO_2-E-imi	1.39	236	2.3
3	Ti-SiO_2-CE-imi	1.43	263	2.3

[a] Amount of imidazolium salt determined by chemical combustion analysis considering the nitrogen percentage.
[b] Determined by DFT method.

125 ppm in the ^{13}C-CP-MAS-NMR spectra (Fig. 4 left) are assigned to the imidazolium moiety [62,63]. The four additional contributions in the aliphatic region can be attributed to the methyl group of the imidazolium moiety and to the propyl chain of the linker connecting the aromatic ring to the silica. ^{29}Si NMR spectra evidence the presence of two signals at -75 ppm and -60 ppm, which can be assigned to $-CH_2$-Si$(OSi)_3$ (T^3) and $-CH_2$-Si$(OSi)_2(OH)$ (T^2) contributions respectively (Fig. 4 right). These signals constitute the proof of the covalent nature of the organic functionalization. The broad band in the region comprised between -115 and -90 ppm can be deconvoluted into three different contributions at -112, -103 and -93 ppm corresponding respectively to Si$(OSi)_4$ (Q^4), Si$(OSi)_3OH$ (Q^3) and Si$(OSi)_2(OH)_2$ (Q^2) species. As expected, the materials submitted to the sole thermal treatment at 550 °C exhibit a higher degree of condensation of the silica network and, therefore, display a more relevant population of Q^4 species (See Figure S5 and Table S1).

The textural properties of the imidazolium functionalized materials were determined using N_2-physisorption (Fig. 5). As expected, the surface functionalization led to a decrease of the BET surface area. The materials treated by extraction (**Ti-SiO_2-E-imi** and **Ti-SiO_2-CE-imi**) exhibited similar specific surface area (Table 2), while the solid obtained via the sole calcination of the structure directing agent (**Ti-SiO_2-C-imi**) revealed a higher specific surface area. This result could be explained

Table 3
Catalytic tests of CO_2 fixation over cyclohexene oxide (CHO) and styrene oxide (SO).

Entry	Epoxide	Catalyst	Epoxide conversion (%)	Cyclic carbonate selectivity (%)	TON [a]	TOF [b]	TON_M [c]	TOF_M [b]
1 [d]	CHO	Ti-SiO_2-C-imi	39	> 95	178	7.4	1009	42
2 [d]	CHO	Ti-SiO_2-CE-imi	41	> 95	134	5.6	2260	94
3 [d]	CHO	Ti-SiO_2-E-imi	63	> 95	217	9.0	4685	195
4 [e]	SO	Ti-SiO_2-E-imi	42	> 95	127	42	938	313
5 [e]	SO	SiO_2-C-imi	34	> 95	94	31	–	–
6 [e]	SO	Ti-SiO_2-E	–	–	–	–	–	–
7 [d]	CHO	XS-Sn-imi [62]	26	> 95	90	3.8	532	22
8 [e]	SO	XS-Sn-imi [62]	32	> 95	96	32	826	275
9 [e]	SO	XS-Zn-imi [62]	32	> 95	98	33	1343	448
10 [d]	CHO	Sn-A-imi(II)-Cl [63]	36	> 95	197	8.2	1341	56
11 [e]	SO	Sn-A-imi(II)-Cl [63]	22	> 95	108	36	735	245
12 [f]	SO	(I-)Meim-UiO-66 [77]	46	71	63	2.6	n.d. [g]	n.d. [g]
13 [h]	SO	ZnTCPP⊂(Br-)Etim-UiO-66 [58]	53	n.d. [g]	56	4.0	n.d. [g]	n.d. [g]
14 [i]	SO	F-IRMOF-3−4d [56]	84	n.d. [g]	589	118	n.d. [g]	n.d. [g]
15 [j]	SO	bV-IMI-NT-2 [39]	22	> 95	103	34	–	–

[a] Turnover number (TON) calculated as moles of epoxide converted / moles of imidazolium sites. Amount of imidazolium salt quantified via chemical combustion analysis for each catalyst and based on %N.
[b] TOF and TOF_M (turnover frequency) calculated respectively as TON and TON_M / reaction time.
[c] TON_M calculated as moles of epoxide converted / moles of metallic sites. Amount of Ti, Sn or Zn quantified via inductively coupled plasma optical emission spectroscopy (ICP-OES) for each catalyst.
[d] Reaction conditions: Cyclohexene oxide CHO (24.0 mL; 237 mmol); mass of catalyst (500 mg); CO_2 initial pressure (25 bar); 150 °C; heating rate (1 °C/min); 24 h; 500 rpm.
[e] Reaction conditions: Styrene oxide SO (24.0 mL; 210 mmol); mass of catalyst (500 mg); CO_2 initial pressure (25 bar); 125 °C; heating rate (1 °C/min); 3 h; 500 rpm.
[f] Temperature (120 °C); CO_2 (1 bar); 24 h; TON calculated considering 46 % of conversion and 71 % of selectivity over 10 mmol of styrene oxide and 50 mg =0.052 mmol of catalyst. [77].
[g] n.d. = not determined.
[h] Temperature (140 °C); CO_2 (constant 1 bar); 14 h; TON calculated considering 52.8 % of yield and 0.95 mol % imidazolium. [58].
[i] Temperature (140 °C); CO_2 (20 bar); 5 h; TON calculated considering 84 % of conversion and a total selectivity over 0.2 mol of styrene oxide and 0.17 g of catalyst with 21.3 wt% of iodine =0.285 mmol. [56].
[j] Temperature (150 °C); CO_2 (40 bar); 3 h. [39].

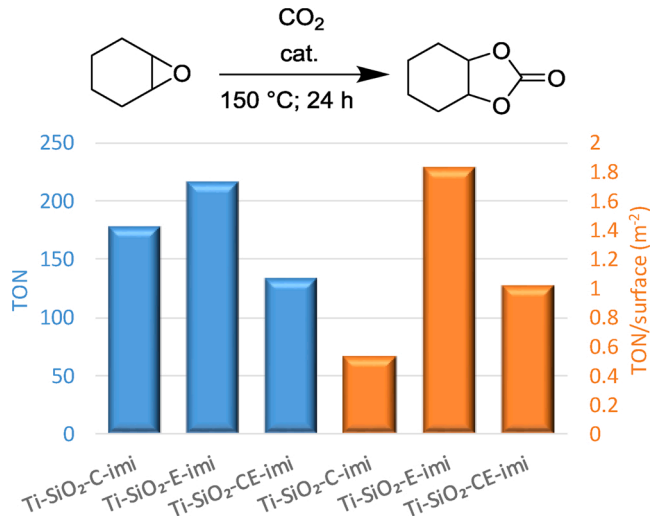

Fig. 6. TON values (blue columns on the left) and TON values normalized by the specific surface area (orange columns on the right) in the catalytic conversion of CO_2 and cyclohexene oxide into the corresponding cyclic carbonate.

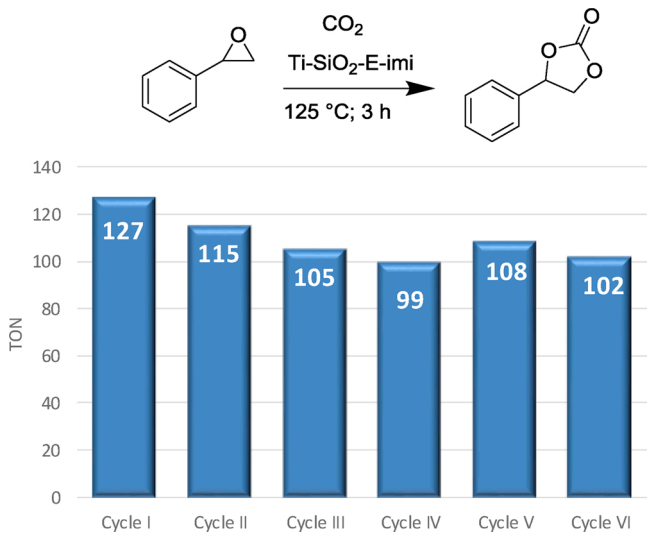

Fig. 7. Recycling tests performed on Ti-SiO_2-E-imi over styrene oxide.

considering the higher amount of free Si−OH group at the surface of the extracted solids (as evidenced from the quantitative ^{29}Si NMR in Figure S5 and Table S1), which can be responsible for a more efficient anchoring of the siloxanes groups and hence for a higher amount of imidazolium species. This hypothesis was confirmed by the quantification of the imidazolium moieties via combustion chemical analysis (Table 2).

3.2. Catalytic conversion of CO_2

All the prepared materials were tested as catalysts in the conversion of carbon dioxide into cyclic carbonates, selecting the challenging reaction between cyclohexene oxide (CHO) and CO_2 as target process. Due to different loading of Ti and imidazolium sites in each material and in order to allow a meaningful comparison between the catalysts, both conversion and turnover number (TON = moles converted / moles of imidazolium) were reported in Table 3 and Fig. 6. Moreover, also turnover numbers calculated considering the Ti loading (TON_M = moles converted / moles of titanium) were included in the table. As can be clearly seen from the data reported in the Table 3, **Ti-SiO_2-E-imi** demonstrated better catalytic performance (Entries 1–3) both in terms of conversion and TON and despite its lower specific surface area [76]. The difference in activity is even more pronounced if the TON are normalized through the BET surface area, as reported on the right part of Fig. 6. This evidence highlights further the importance of the insertion of titanium as single site in the silica network.

Ti-SiO_2-E-imi revealed good activity also when tested over another challenging epoxide as styrene oxide (SO) (Entry 4). It is important to mention that the reaction was performed at a lower temperature (compared to standard tests usually employing 150 °C) and at a short reaction time (3 h). A Ti-free material was tested under the same condition (Entry 5) exhibiting a conversion of 34 % and a TON of 94. It emphasizes once more the importance of the insertion of Ti in the structure. A test with the **Ti-SiO_2-E** is reported at Entry 6. No cyclic carbonate was detected using the ^{1}H-NMR and the monitoring of the pressure (Figure S6) revealed no consumption of the CO_2. These results evidence the imidazolium chloride is the main catalyst while the Ti is its co-catalyst. The activity of **Ti-SiO_2-E-imi** was also compared with literature data. For this purpose, it deserves to be mentioned that a direct comparison with reference catalysts is often hindered by the different reaction conditions in terms of pressure, temperature, reaction time, nature of the nucleophile and presence of solvents, amongst others. Moreover, many authors report the use of Lewis acid heterogeneous catalysts in presence of ammonium or imidazolium salts in homogeneous conditions. In Table 3, we compare our materials with other silica-based catalysts previously reported by us (hence tested exactly under the same reaction conditions) or some fully heterogeneous catalysts reported in literature. Importantly **Ti-SiO_2-E-imi** revealed improved catalytic performances in terms of TON compared to previously reported catalysts containing tin or zinc inserted as single sites in a mesoporous silica structure as XS-Sn-imi [62] (compare entries 3 vs 7 and entries 4 vs 8) and XS-*Zn*-imi [62] (compare entries 4 vs 9). More significantly, **Ti-SiO_2-E-imi** is more active than the multifunctional solid Sn-A-imi (II)-Cl [63] (compare entries 3−4 vs 10–11), which presents imidazolium chloride catalytic sites together with both Lewis acids sites and H-donor as co-catalysts. This demonstrates the important role of titanium as Lewis acid co-catalysts.

Moreover, **Ti-SiO_2-E-imi** displayed higher TON and TOF than a MOF based system (Entry 12) functionalized with imidazolium moieties (hence fully heterogeneous). It should be noted that the catalyst reported in Entry 12 operates at slightly lower temperature (120 °C) and pressure (1 bar) but it presents a different nucleophile (iodide compared with chloride in our system). A similar strategy was employed by Liang et al., who reported the use of a bi-functional catalyst bearing Zn as Lewis acid and functionalized with imidazolium bromide (Entry 13). This last example displayed lower activity than our material despite the higher reaction temperature and the use of bromide as nucleophile [58]. The increased performance of the bifunctional MOF reported in Entry 14 can be attributed to the presence of the ammonium iodide as catalytically active specie together with the more elevate reaction temperature (140 °C compared with 125 °C in our case). As expected, Ti-SiO_2-E solid shows better carbonate yield than some other highly performing catalysts presenting only imidazolium-based units and used in absence of co-catalytically active species (Entry 15).

The reusability of the **Ti-SiO_2-E-imi** catalyst was tested over several cycles in the presence of styrene oxide. The reaction conditions were selected in order to ensure a catalyst performance far enough from total conversion [76]. After each cycle, the material was washed with toluene and ethanol, dried and employed in a successive cycle without further activation. As can be seen in Fig. 7, the activity of **Ti-SiO_2-E-imi** was preserved in consecutives runs, only a slight decrease was evidenced in the initial cycles followed by a stabilization (starting from the 3rd run). This initial decrease could be ascribed to the presence of minor amount of cyclic carbonates strongly adsorbed on the catalyst surface (see Figure S7).

The wide applicability of the **Ti-SiO_2-E-Imi** catalyst was evidenced

Table 4
Conversion of various epoxides using **Ti-SiO$_2$-E-imi.**

Entry	Substrate	Temperature (°C)	Time (h)	Conv. (%)	Sel. (%)
1	Styrene oxide	125	3	42	> 95
2	1,2-Epoxybutane	125	3	41	> 95
3	Epichlorohydrin	100	3	53	> 95
4	Glycidol	50	6	28	> 95
5 [a]	Glycidol	50	6	22	> 95

Reaction conditions: Substrate (24.0 mL); mass of catalyst (500 mg); CO_2 initial pressure (25 bar); heating rate (1 °C/min); 500 rpm.
[a] Constant pressure (5 ± 0.5 bar).

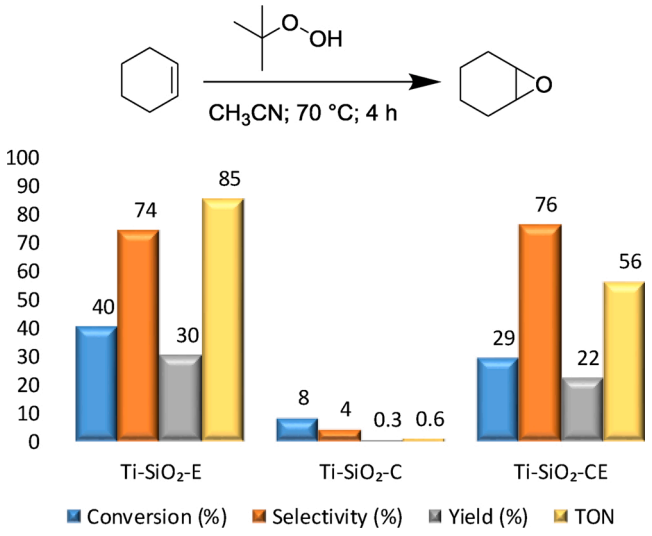

Fig. 8. Catalytic results for the epoxidation of cyclohexene. Reaction conditions: alkene (4.5 mmol), $TBHP_{aq}$ (4.5 mmol), catalyst (100 mg), acetonitrile as solvent (4.5 mL), temperature 70 °C, reaction time 4 h.

by running the reaction in the presence of other epoxides (Table 4). An additional test over the 1,2-epoxybutane (Entry 2) was performed at 125 °C. This experiment further supports the ability of the Ti centre to activate the oxirane ring. As expected, lower temperatures can be used in presence of more reactive epoxides like epichlorohydrin (Entry 3) or glycidol (Entry 4). The use of glycidol allows decreasing the reaction temperature down to 50 °C (Entry 4). The same experiment was reproduced using a constant pressure of 5 bars (Entry 5) demonstrating only a minor influence of the CO_2 pressure on the conversion. It should be highlighted that the selectivity was always close to 100 % and no by-product was observed from ^{1}H NMR analysis of the reaction mixture. The regular decrease of pressure in the reactor due to CO_2 consumption was monitored over the time (see Figure S8).

These results prove that **Ti-SiO$_2$-E-imi** is an efficient and versatile catalyst in the CO_2 conversion, able to preserve its activity in multiple cycles. Moreover, the **Ti-SiO$_2$-E** matrix can be synthetized in aqueous medium with a short synthesis procedure not requiring thermal treatments under static conditions and the release of the porosity can be achieved via simple extraction. All these parameters contribute in making the entire process highly sustainable.

3.3. Epoxidation reaction

Moreover, the proposed solid could present other additional advantages. It is known that Ti-silicates are amongst the most active catalysts in epoxidation reactions [21–27]. In this reaction, the Ti centres play the role of Lewis acids interacting with the peroxides. To prove that the efficiency of the materials synthesized can be dual, preliminary tests were performed selecting as target reaction the epoxidation of cyclohexene into cyclohexene oxide using tert-butyl hydroperoxide (TBHP) as oxidant (Fig. 8). The best catalytic performance was achieved employing the **Ti-SiO$_2$-E** catalyst. This result is ascribed to the almost complete insertion of Ti in tetrahedral coordination. As expected, **Ti-SiO$_2$-C** showed poor activity and the main products obtained are side-products (identified as cyclohex-2-en-1-one and cyclohex-2-en-1-ol) while **Ti-SiO$_2$-CE** exhibits intermediate conversion.

Ti-SiO$_2$-E displayed good performances also when compared with other reference catalysts already reported in literature. A hybrid mesoporous titanosilicate (19 %Me-Ti-MCM-41) prepared by Lin et al. [69] demonstrated similar conversion (38.5 %) and a higher selectivity (94.1 %) after 5 h reaction, attributed to the more hydrophobic surface. Recently, Wang and Balkus [78] published interesting results combining a conversion of 22 % in 2 h with excellent selectivity (94 %) using reaction conditions close to the ones adopted by us. It should be noted that our best solid catalyst displays a twice higher conversion. Wang et al. [79] also published the synthesis of an extra-large-pore zeolites Ti-SSZ-53 able to achieve competitive results with excellent selectivity (94.6 %) but lower conversion (12.2 %) after 4 h. It should be mentioned that the epoxidation reactions with **Ti-SiO$_2$-E** were always performed in presence of an aqueous solution of *tert*-butyl hydroperoxide (TBHP) while the other reported examples employ non-aqueous TBHP solution which can account for the higher selectivity [19,80,81].

3.4. Towards a cascade reaction

The above described results demonstrated the efficiency of **Ti-SiO$_2$-E** and **Ti-SiO$_2$-E-imi** as catalysts in the epoxidation of cyclohexene to cyclohexene oxide and the carbonatation of cyclohexene oxide, respectively. Hence, to challenge even more our catalyst we decided to test them in the two consecutive reactions. Table 5 summarizes a series of preliminary tests performed as proof of principle. Entry 1 displays the CHO yield achieved in the presence of 100 mg of **Ti-SiO$_2$-E.** As expected, a decrease of the amount of catalyst (Entry 2) caused a lowering of the yield. This result was also accompanied by a decrease of the selectivity. A catalytic essay in the presence of **Ti-SiO$_2$-E-imi** revealed a drastic drop of the catalytic performance (Entry 3). No epoxidation product was observed even after 24 h reaction. The side products were identified as cyclohex-2-en-1-one and cyclohex-2-en-1-ol. This result could be ascribed to the hydrophilic nature of the imidazolium moieties, which can decrease the possibility of interaction with the hydrophobic cyclic alkene [82]. To circumvent this problem, a physical mixture of both **Ti-SiO$_2$-E** and **Ti-SiO$_2$-E-imi** (Entry 4) was employed. The idea is to have a solid with two components in which one partner can act as catalyst for the epoxidation while the second will convert the epoxide, as depicted in Scheme 2. Interestingly, the yield in CHO was slightly higher [69,82,83] thus proving that the presence of **Ti-SiO$_2$-E-imi** has no detrimental effect on the epoxidation reaction. The same catalysts mixture constituted by 50 wt% of **Ti-SiO2**-E and 50 wt% of **Ti-SiO$_2$-E-imi** was successfully used in the conversion of carbon dioxide (reaction 2; Entry 5) and a result similar to the one obtained with the sole **Ti-SiO$_2$-E-imi** (Entry 6) proves that there is no detrimental effect in CO_2 conversion by using the mixture of both catalysts. The results obtained demonstrate that the catalytic mixture can be used for both processes (reaction 1 and 2) without decreasing the overall catalysts performances. Moreover, these

Table 5
Cascade Reaction.

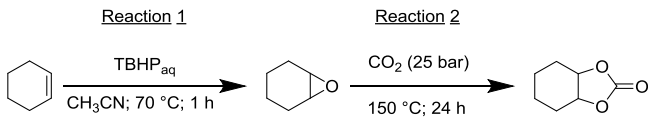

Entry	Reaction	Catalyst	Conv. (%)	Sel. (%)	Yield (%)
1	1	Ti-SiO$_2$-E (100 mg)	45	74	33
2	1	Ti-SiO$_2$-E (50 mg)	30	47	14
3	1	Ti-SiO$_2$-E-imi (50 mg)	17	–	–
4	1	Ti-SiO$_2$-E-imi (50 mg) + Ti-SiO$_2$-E (50 mg)	33	79	26
5	2	Ti-SiO$_2$-E-imi (250 mg) + Ti-SiO$_2$-E (250 mg)	34	> 95	32
6	2	Ti-SiO$_2$-E-imi (250 mg)	33	> 95	31

Reaction 1: Cyclohexene (4.5 mmol); TBHP$_{aq.}$ 70 % (4.5 mmol); acetonitrile (4.5 mL); mesitylene as internal standard (50 μL); temperature (70 °C); 1 h.
Reaction 2: Cyclohexene oxide (24.0 mL; 237 mmol); CO_2 initial pressure (25 bar); 150 °C; heating rate (1 °C/min); 24 h; 500 rpm.

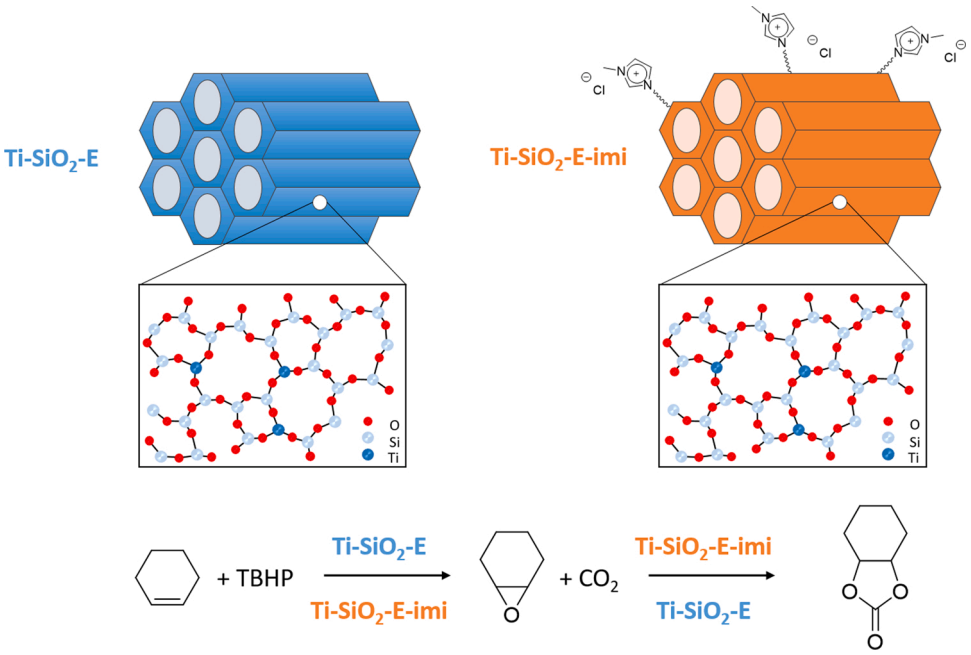

Scheme 2. Representation of the two catalytic reaction.

tests highlight the importance of the spatial proximity of the catalyst (imidazolium chloride) and the co-catalyst (Ti centre) in the formation of cyclic carbonates.

4. Conclusion

Porous titanosilicate nanospheres were efficiently prepared via a straightforward synthesis protocol requiring only 1 h reaction and no hydrothermal treatment under static conditions thus strongly decreasing the energy consumption. The effect of the post-synthetic treatment on the insertion of titanium was investigated, proving that the pores can be freed from the template through an extraction in aqueous medium. The solids were functionalized with imidazolium moieties and thoroughly characterized via various techniques including transmission electron microscopy, N_2 physisorption, XPS, UV–vis, ^{13}C and ^{29}Si solid state NMR. The bifunctional particles were successfully employed as catalysts in the conversion of carbon dioxide with various epoxides to form the corresponding cyclic carbonates. The results obtained proved the added value of a titanium containing support which plays the role of Lewis acid enhancing the overall catalytic performance. The best solid displayed better performances in terms of TON and TOF than other fully heterogeneous catalysts reported in literature. The catalytic performance correlate coherently with all the set of characterization data. Moreover, the catalyst was reused in multiple cycle without decrease of the catalyst performance. The bifunctional nature of the best solid was challenged testing the catalyst in the epoxidation reaction of cyclohexene. The same catalytic mixture, composed by the titanosilicate nanospheres and bifunctional solid, was used to convert the cyclohexene into cyclohexene oxide and subsequently the cyclohexene oxide into the corresponding carbonate. All these results prove the versatility of the catalysts and confirm the key role played by the Ti centre inserted in tetrahedral coordination.

CRediT authorship contribution statement

Adrien Comès: Investigation, Writing - original draft, Visualization. **Rémy Poncelet:** Investigation. **Paolo P. Pescarmona:** Conceptualization, Writing - review & editing. **Carmela Aprile:** Conceptualization, Writing - review & editing, Supervision, Funding acquisition.

Declaration of Competing Interest

The authors declare that they have no known competing financial interests or personal relationships that could have appeared to influence

the work reported in this paper.

Acknowledgements

A. Comès acknowledges the University of Namur for a PhD fellowship. The authors acknowledge FNRS trough the FNRS-EQPU.N034.17 F and the FNRS-GEQ-U.G014.19 for the financial support. This research used resources of the "Plateforme Technologique Physico-Chemical Characterisation" – PC^2. This research also used resources of the Electron Microscopy Service located at the University of Namur. This Service is member of the "Plateforme Technologique Morphologie – Imagerie". The authors thank Dr. Luca Fusaro for his support in NMR measurements and Dr. Alexandre Felten in XPS measurements.

Appendix A. Supplementary data

Supplementary material related to this article can be found, in the online version, at doi:https://doi.org/10.1016/j.jcou.2021.101529.

References

[1] P.T. Anastas, J.C. Warner, Green Chemistry: Theory and Practice, Oxford University Press, Oxford, 1998.
[2] R.A. Sheldon, I.W.C.E. Arends, U. Hanefeld, Green Chemistry and Catalysis, 2007.
[3] M. Poliakoff, J.M. Fitzpatrick, T.R. Farren, P.T. Anastas, Green chemistry: science and politics of change, Science 297 (5582) (2002) 807–810.
[4] R.A. Sheldon, Metrics of green chemistry and sustainability: past, present, and future, ACS Sustain. Chem. Eng. 6 (1) (2017) 32–48.
[5] M. Appl, Ammonia, 2. Production Processes, Ullmann's Encyclopedia of Industrial Chemistry, 2011.
[6] G. Cecchin, G. Morini, F. Piemontesi, Ziegler-Natta Catalysts, Kirk-Othmer Encyclopedia of Chemical Technology, 2003.
[7] C.T. Kresge, M.E. Leonowicz, W.J. Roth, J.C. Vartuli, J.S. Beck, Ordered mesoporous molecular sieves synthesized by a liquid-crystal template mechanism, Nature 359 (6397) (1992) 710–712.
[8] J.S. Beck, J.C. Vartuli, W.J. Roth, M.E. Leonowicz, C.T. Kresge, K.D. Schmitt, C.T. W. Chu, D.H. Olson, E.W. Sheppard, S.B. McCullen, J.B. Higgins, J.L. Schlenker, A new family of mesoporous molecular sieves prepared with liquid crystal templates, J. Am. Chem. Soc. 114 (27) (1992) 10834–10843.
[9] D. Zhao, J. Feng, Q. Huo, N. Melosh, G.H. Fredrickson, B.F. Chmelka, G.D. Stucky, Triblock copolymer syntheses of mesoporous silica with periodic 50 to 300 angstrom pores, Science 279 (5350) (1998) 548–552.
[10] A. Taguchi, F. Schüth, Ordered mesoporous materials in catalysis, Microporous Mesoporous Mater. 77 (1) (2005) 1–45.
[11] R. Xu, W. Pang, J. Yu, Q. Huo, J. Chen, Chemistry of Zeolites and Related Porous Materials, Wiley, 2007.
[12] X. Collard, L. Li, W. Lueangchaichaweng, A. Bertrand, C. Aprile, P.P. Pescarmona, Ga-MCM-41 nanoparticles: synthesis and application of versatile heterogeneous catalysts, Catal. Today 235 (2014) 184–192.
[13] L. Li, X. Collard, A. Bertrand, B.F. Sels, P.P. Pescarmona, C. Aprile, Extra-small porous Sn-silicate nanoparticles as catalysts for the synthesis of lactates, J. Catal. 314 (2014) 56–65.
[14] X. Collard, P. Louette, S. Fiorilli, C. Aprile, High surface area zincosilicates as efficient catalysts for the synthesis of ethyl lactate: an in-depth structural investigation, Phys. Chem. Chem. Phys. 17 (40) (2015) 26756–26765.
[15] N. Godard, A. Vivian, L. Fusaro, L. Cannavicci, C. Aprile, D.P. Debecker, High-yield synthesis of ethyl lactate with mesoporous tin silicate catalysts prepared by an aerosol-assisted sol-gel process, Chem. Cat. Chem. 9 (12) (2017) 2211–2218.
[16] P.J. Cordeiro, P. Guillo, C.S. Spanjers, J.W. Chang, M.I. Lipschutz, M.E. Fasulo, R. M. Rioux, T.D. Tilley, Titanium–Germoxy precursor route to germanium-modified epoxidation catalysts with enhanced activity, ACS Catal. 3 (10) (2013) 2269–2279.
[17] N.M. Schweitzer, B. Hu, U. Das, H. Kim, J. Greeley, L.A. Curtiss, P.C. Stair, J. T. Miller, A.S. Hock, Propylene hydrogenation and propane dehydrogenation by a single-site Zn2+ on silica catalyst, ACS Catal. 4 (4) (2014) 1091–1098.
[18] F. Berube, A. Khadraoui, J. Florek, S. Kaliaguine, F. Kleitz, A generalized method toward high dispersion of transition metals in large pore mesoporous metal oxide/silica hybrids, J. Colloid Interface Sci. 449 (2015) 102–114.
[19] M. Fukuda, N. Tsunoji, Y. Yagenji, Y. Ide, S. Hayakawa, M. Sadakane, T. Sano, Highly active and selective Ti-incorporated porous silica catalysts derived from grafting of titanium(iv)acetylacetonate, J. Mater. Chem. A 3 (29) (2015) 15280–15291.
[20] W. Lueangchaichaweng, N.R. Brooks, S. Fiorilli, E. Gobechiya, K. Lin, L. Li, S. Parres-Esclapez, E. Javon, S. Bals, G. Van Tendeloo, J.A. Martens, C. E. Kirschhock, P.A. Jacobs, P.P. Pescarmona, Gallium oxide nanorods: novel, template-free synthesis and high catalytic activity in epoxidation reactions, Angew. Chem. Int. Ed. Engl. 53 (6) (2014) 1585–1589.
[21] V. Smeets, E.M. Gaigneaux, D.P. Debecker, Hierarchical micro-/macroporous TS-1 zeolite epoxidation catalyst prepared by steam assisted crystallization, Microporous Mesoporous Mater. 293 (2020).
[22] T. Blasco, Synthesis, Characterization, and Catalytic Activity of Ti-MCM-41 Structures, J. Catal. 156 (1) (1995) 65–74.
[23] K. Lin, P. Pescarmona, H. Vandepitte, D. Liang, G. Vantendeloo, P. Jacobs, Synthesis and catalytic activity of Ti-MCM-41 nanoparticles with highly active titanium sites, J. Catal. 254 (1) (2008) 64–70.
[24] M. Guidotti, C. Pirovano, N. Ravasio, B. Lázaro, J.M. Fraile, J.A. Mayoral, B. Coq, A. Galarneau, The use of H2O2 over titanium-grafted mesoporous silica catalysts: a step further towards sustainable epoxidation, Green Chem. 11 (9) (2009) 1421.
[25] F. Bérubé, A. Khadhraoui, M.T. Janicke, F. Kleitz, S. Kaliaguine, Optimizing silica synthesis for the preparation of mesoporous Ti-SBA-15 epoxidation catalysts, Ind. Eng. Chem. Res. 49 (15) (2010) 6977–6985.
[26] F. Bérubé, B. Nohair, F. Kleitz, S. Kaliaguine, Controlled postgrafting of titanium chelates for improved synthesis of Ti-SBA-15 epoxidation catalysts, Chem. Mater. 22 (6) (2010) 1988–2000.
[27] B. Samran, S. Aungkutranont, T.J. White, S. Wongkasemjit, Room temperature synthesis of Ti-SBA-15 from silatrane and titanium-glycolate and its catalytic performance towards styrene epoxidation, J. Solgel Sci. Technol. 57 (2) (2010) 221–228.
[28] A. Corma, H. Garcia, Lewis acids: from conventional homogeneous to green homogeneous and heterogeneous catalysis, Chem. Rev. 103 (11) (2003) 4307–4365.
[29] M.J. Cordon, Consequences of the Hydrophobicity and Spatial Constraints of Confining Environments in Lewis Acid Zeolites for Aqueous-phase Glucose Isomerization Catalysis, Purdue University, West Lafayette, Indianna, 2018, p. 424.
[30] D.T. Bregante, A.M. Johnson, A.Y. Patel, E.Z. Ayla, M.J. Cordon, B.C. Bukowski, J. Greeley, R. Gounder, D.W. Flaherty, Cooperative effects between hydrophilic pores and solvents: catalytic consequences of hydrogen bonding on alkene epoxidation in zeolites, J. Am. Chem. Soc. 141 (18) (2019) 7302–7319.
[31] V. Smeets, C. Boissière, C. Sanchez, E.M. Gaigneaux, E. Peeters, B.F. Sels, M. Dusselier, D.P. Debecker, Aerosol route to TiO2–SiO2 catalysts with tailored pore architecture and high epoxidation activity, Chem. Mater. 31 (5) (2019) 1610–1619.
[32] M. Pitínová-Štekrová, P. Eliášová, T. Weissenberger, M. Shamzhy, Z. Musilová, J. Čejka, Highly selective synthesis of campholenic aldehyde over Ti-MWW catalysts by α-pinene oxide isomerization, Catal. Sci. Technol. 8 (18) (2018) 4690–4701.
[33] S. Ammaji, G.S. Rao, K.V.R. Chary, Acetalization of glycerol with acetone over various metal-modified SBA-15 catalysts, Appl. Petrochem. Res. 8 (2) (2018) 107–118.
[34] M.J. Cordon, J.W. Harris, J.C. Vega-Vila, J.S. Bates, S. Kaur, M. Gupta, M. E. Witzke, E.C. Wegener, J.T. Miller, D.W. Flaherty, D.D. Hibbitts, R. Gounder, Dominant Role of Entropy in Stabilizing Sugar Isomerization Transition States within Hydrophobic Zeolite Pores, J. Am. Chem. Soc. 140 (43) (2018) 14244–14266.
[35] S. Baj, T. Krawczyk, K. Jasiak, A. Siewniak, M. Pawlyta, Catalytic coupling of epoxides and CO_2 to cyclic carbonates by carbon nanotube-supported quaternary ammonium salts, Appl. Catal. A Gen. 488 (2014) 96–102.
[36] J. Steinbauer, C. Kubis, R. Ludwig, T. Werner, Mechanistic study on the addition of CO_2 to epoxides catalyzed by ammonium and phosphonium salts: a combined spectroscopic and kinetic approach, ACS Sustain. Chem. Eng. 6 (8) (2018) 10778–10788.
[37] W. Wang, Y. Wang, C. Li, L. Yan, M. Jiang, Y. Ding, State-of-the-Art multifunctional heterogeneous POP catalyst for cooperative transformation of CO_2 to cyclic carbonates, ACS Sustain. Chem. Eng. 5 (6) (2017) 4523–4528.
[38] M. Buaki-Sogo, H. Garcia, C. Aprile, Imidazolium-based silica microreactors for the efficient conversion of carbon dioxide, Catal. Sci. Technol. 5 (2) (2015) 1222–1230.
[39] M. Buaki-Sogó, A. Vivian, L.A. Bivona, H. García, M. Gruttadauria, C. Aprile, Imidazolium functionalized carbon nanotubes for the synthesis of cyclic carbonates: reducing the gap between homogeneous and heterogeneous catalysis, Catal. Sci. Technol. 6 (24) (2016) 8418–8427.
[40] Z. Zhang, F. Fan, H. Xing, Q. Yang, Z. Bao, Q. Ren, Efficient synthesis of cyclic carbonates from atmospheric CO_2 using a positive charge delocalized ionic liquid catalyst, ACS Sustain. Chem. Eng. 5 (4) (2017) 2841–2846.
[41] J. Tharun, A.C. Kathalikkattil, R. Roshan, D.-H. Kang, H.-C. Woo, D.-W. Park, Microwave-assisted, rapid cycloaddition of allyl glycidyl ether and CO_2 by employing pyridinium-based ionic liquid catalysts, Catal. Commun. 54 (2014) 31–34.
[42] W. Cheng, X. Chen, J. Sun, J. Wang, S. Zhang, SBA-15 supported triazolium-based ionic liquids as highly efficient and recyclable catalysts for fixation of CO_2 with epoxides, Catal. Today 200 (2013) 117–124.
[43] L.J. Zhou, W. Sun, N.N. Yang, P. Li, T. Gong, W.J. Sun, Q. Sui, E.Q. Gao, A facile and versatile "Click" approach toward multifunctional ionic metal-organic frameworks for efficient conversion of CO2, Chem. Sus. Chem. 12 (10) (2019) 2202–2210.
[44] C. Claver, M.B. Yeamin, M. Reguero, A.M. Masdeu-Bultó, Recent advances in the use of catalysts based on natural products for the conversion of CO2 into cyclic carbonates, Green Chem. 22 (22) (2020) 7665–7706.
[45] T. Ema, Y. Miyazaki, J. Shimonishi, C. Maeda, J.Y. Hasegawa, Bifunctional porphyrin catalysts for the synthesis of cyclic carbonates from epoxides and CO2: structural optimization and mechanistic study, J. Am. Chem. Soc. 136 (43) (2014) 15270–15279.
[46] M. Taherimehr, B. Van de Voorde, L.H. Wee, J.A. Martens, D.E. De Vos, P. P. Pescarmona, Strategies for enhancing the catalytic performance of metal-organic frameworks in the fixation of CO2 into cyclic carbonates, Chem. Sus. Chem. 10 (6) (2017) 1283–1291.

[47] A.J. Kamphuis, F. Milocco, L. Koiter, P.P. Pescarmona, E. Otten, Highly selective single-component formazanate ferrate(II) catalysts for the conversion of CO_2 into cyclic carbonates, Chem. Sus. Chem. 12 (15) (2019) 3635–3641.
[48] J. Liang, Y.-B. Huang, R. Cao, Metal–organic frameworks and porous organic polymers for sustainable fixation of carbon dioxide into cyclic carbonates, Coord. Chem. Rev. 378 (2019) 32–65.
[49] L.G. Ding, B.J. Yao, W.L. Jiang, J.T. Li, Q.J. Fu, Y.A. Li, Z.H. Liu, J.P. Ma, Y. B. Dong, Bifunctional imidazolium-based ionic liquid decorated UiO-67 type MOF for selective CO2 adsorption and catalytic property for CO2 cycloaddition with epoxides, Inorg. Chem. 56 (4) (2017) 2337–2344.
[50] C. Calabrese, F. Giacalone, C. Aprile, Hybrid catalysts for CO_2 conversion into cyclic carbonates, Catalysts 9 (4) (2019).
[51] M. North, P. Villuendas, C. Young, A gas-phase flow reactor for ethylene carbonate synthesis from waste carbon dioxide, Chemistry 15 (43) (2009) 11454–11457.
[52] J. Melendez, M. North, P. Villuendas, One-component catalysts for cyclic carbonate synthesis, Chem. Commun. (Camb.) 0 (18) (2009) 2577–2579.
[53] J. Melendez, M. North, P. Villuendas, C. Young, One-component bimetallic aluminium(salen)-based catalysts for cyclic carbonate synthesis and their immobilization, Dalton Trans. 40 (15) (2011) 3885–3902.
[54] M. North, P. Villuendas, Influence of support and linker parameters on the activity of silica-supported catalysts for cyclic carbonate synthesis, Chem. Cat. Chem. 4 (6) (2012) 789–794.
[55] S.M. Sadeghzadeh, A heteropolyacid-based ionic liquid immobilized onto fibrous nano-silica as an efficient catalyst for the synthesis of cyclic carbonate from carbon dioxide and epoxides, Green Chem. 17 (5) (2015) 3059–3066.
[56] X. Zhou, Y. Zhang, X. Yang, L. Zhao, G. Wang, Functionalized IRMOF-3 as efficient heterogeneous catalyst for the synthesis of cyclic carbonates, J. Mol. Catal. A Chem. 361-362 (2012) 12–16.
[57] D. Ma, B. Li, K. Liu, X. Zhang, W. Zou, Y. Yang, G. Li, Z. Shi, S. Feng, Bifunctional MOF heterogeneous catalysts based on the synergy of dual functional sites for efficient conversion of CO2 under mild and co-catalyst free conditions, J. Mater. Chem. A 3 (46) (2015) 23136–23142.
[58] J. Liang, Y.Q. Xie, Q. Wu, X.Y. Wang, T.T. Liu, H.F. Li, Y.B. Huang, R. Cao, Zinc Porphyrin/Imidazolium integrated multivariate zirconium metal-organic frameworks for transformation of CO_2 into cyclic carbonates, Inorg. Chem. 57 (5) (2018) 2584–2593.
[59] J.F. Kurisingal, Y. Rachuri, R.S. Pillai, Y. Gu, Y. Choe, D.W. Park, Ionic-liquid-Functionalized UiO-66 framework: an experimental and theoretical study on the cycloaddition of CO2 and epoxides, Chem. Sus. Chem. 12 (5) (2019) 1033–1042.
[60] J. Liang, Y.Q. Xie, X.S. Wang, Q. Wang, T.T. Liu, Y.B. Huang, R. Cao, An imidazolium-functionalized mesoporous cationic metal-organic framework for cooperative CO2 fixation into cyclic carbonate, Chem. Commun. (Camb.) 54 (4) (2018) 342–345.
[61] M. Ding, H.-L. Jiang, Incorporation of imidazolium-based poly(ionic liquid)s into a metal–Organic framework for CO2 capture and conversion, ACS Catal. (2018) 3194–3201.
[62] A. Comès, X. Collard, L. Fusaro, L. Atzori, M.G. Cutrufello, C. Aprile, Bi-functional heterogeneous catalysts for carbon dioxide conversion: enhanced performances at low temperature, RSC Adv. 8 (45) (2018) 25342–25350.
[63] A. Comès, S. Fiorilli, C. Aprile, Multifunctional heterogeneous catalysts highly performing in the conversion of carbon dioxide: mechanistic insights, J. Co2 Util. 37 (2020) 213–221.
[64] N. Godard, X. Collard, A. Vivian, L.A. Bivona, S. Fiorilli, L. Fusaro, C. Aprile, Rapid room temperature synthesis of tin-based mesoporous solids: influence of the particle size on the production of ethyl lactate, Appl. Catal. A Gen. 556 (2018) 73–80.
[65] B. Sorée, Synthèse De Liquides Ioniques Supportés Pour La Conception De Catalyseurs Actifs Dans La Fixation Chimique Du Dioxyde De Carbone, Faculté Des Sciences, Facultés Universitaires Notre-Dame de la Paix de Namur, Namur, 2012, p. 86.
[66] J. Kecht, A. Schlossbauer, T. Bein, Selective functionalization of the outer and inner surfaces in mesoporous silica nanoparticles, Chem. Mater. 20 (23) (2008) 7207–7214.
[67] X. Collard, A. Comès, C. Aprile, Mesoporous metal oxide/silica composites with photocatalytic activity and magnetic response, Catal. Today 241 (2015) 33–39.
[68] M. Thommes, K. Kaneko, A.V. Neimark, J.P. Olivier, F. Rodriguez-Reinoso, J. Rouquerol, K.S.W. Sing, Physisorption of gases, with special reference to the evaluation of surface area and pore size distribution (IUPAC Technical Report), Pure Appl. Chem. 87 (9-10) (2015) 1051–1069.
[69] K. Lin, P.P. Pescarmona, K. Houthoofd, D. Liang, G. Van Tendeloo, P.A. Jacobs, Direct room-temperature synthesis of methyl-functionalized Ti-MCM-41 nanoparticles and their catalytic performance in epoxidation, J. Catal. 263 (1) (2009) 75–82.
[70] F. Carniato, C. Bisio, L. Sordelli, E. Gavrilova, M. Guidotti, Ti-POSS covalently immobilized onto mesoporous silica: a model for active sites in heterogeneous catalytic epoxidation, Inorganica Chim. Acta 380 (1) (2012) 244–251.
[71] M. Guidotti, I. Batonneau-Gener, E. Gianotti, L. Marchese, S. Mignard, R. Psaro, M. Sgobba, N. Ravasio, The effect of silylation on titanium-containing silica catalysts for the epoxidation of functionalised molecules, Microporous Mesoporous Mater. 111 (1-3) (2008) 39–47.
[72] M.S. Morey, S. O'Brien, S. Schwarz, G.D. Stucky, Hydrothermal and postsynthesis surface modification of cubic, MCM-48, and ultralarge pore SBA-15 mesoporous silica with titanium, Chem. Mater. 12 (4) (2000) 898–911.
[73] I. Grohmann, W. Pilz, G. Walther, H. Kosslick, V.A. Tuan, XPS-investigation of titanium modified MFI-type zeolites, Surf. Interface Anal. 22 (1-12) (1994) 403–406.
[74] Z. Luan, E.M. Maes, P.A.W. van der Heide, D. Zhao, R.S. Czernuszewicz, L. Kevan, Incorporation of titanium into mesoporous silica molecular sieve SBA-15, Chem. Mater. 11 (12) (1999) 3680–3686.
[75] C. Liu, J. Huang, D. Sun, Y. Zhou, X. Jing, M. Du, H. Wang, Q. Li, Anatase type extra-framework titanium in TS-1: a vital factor influencing the catalytic activity toward styrene epoxidation, Appl. Catal. A Gen. 459 (2013) 1–7.
[76] F. Schüth, M.D. Ward, J.M. Buriak, Common pitfalls of catalysis manuscripts submitted to chemistry of materials, Chem. Mater. 30 (11) (2018) 3599–3600.
[77] J. Liang, R.P. Chen, X.Y. Wang, T.T. Liu, X.S. Wang, Y.B. Huang, R. Cao, Postsynthetic ionization of an imidazole-containing metal-organic framework for the cycloaddition of carbon dioxide and epoxides, Chem. Sci. 8 (2) (2017) 1570–1575.
[78] Z. Wang, K.J. Balkus, Synthesis and modification of titanium containing wrinkled mesoporous silica for cyclohexene epoxidation, Microporous Mesoporous Mater. 243 (2017) 76–84.
[79] J.-G. Wang, H. Wang, T. Yokoi, T. Tatsumi, Synthesis of Ti-containing extra-large-pore zeolites of Ti-CIT-5 and Ti-SSZ-53 and their catalytic applications, Microporous Mesoporous Mater. 276 (2019) 207–212.
[80] I. del Hierro, Y. Pérez, M. Fajardo, Heterogenization of titanium(IV) complexes with amine bis(phenolate) ligands onto SBA-15: exploring their catalytic epoxidation and electrochemical behaviour, Appl. Organomet. Chem. 30 (4) (2016) 208–214.
[81] X. Ouyang, S.-J. Hwang, D. Xie, T. Rea, S.I. Zones, A. Katz, Heteroatom-substituted delaminated zeolites as solid lewis acid catalysts, ACS Catal. 5 (5) (2015) 3108–3119.
[82] J. Silvestre-Alberó, M.E. Domine, J.L. Jordá, M.T. Navarro, F. Rey, F. Rodríguez-Reinoso, A. Corma, Spectroscopic, calorimetric, and catalytic evidences of hydrophobicity on Ti-MCM-41 silylated materials for olefin epoxidations, Appl. Catal. A Gen. 507 (2015) 14–25.
[83] L.E. Manangon-Perugachi, A. Vivian, P. Eloy, D.P. Debecker, C. Aprile, E. M. Gaigneaux, Hydrophobic titania-silica mixed oxides for the catalytic epoxidation of cyclooctene, Catal. Today (2019).